A Fully Integrated Biosensing Platform Combining Acoustofluidics and Electromagnetic Metamaterials

S. Zahertar,[1] Y. Wang,[2] R.Tao,[1] J. Xie,[2] Y.Q. Fu,[1] H. Torun[1,*]

[1]Faculty of Engineering and Environment, Northumbria University, Newcastle upon Tyne, NE1 8ST, UK

[2] The State Key Laboratory of Fluid Power and Mechatronic Systems, Zhejiang University, Hangzhou 310027, China

* Corresponding author: Hamdi Torun, hamdi.torun@northumbria.ac.uk

Abstract

A key challenge in biosensing technology is to develop integrated approaches with the multiple capabilities of bio-sampling, fluid manipulation, high-precision detection and wireless operation. In this work, we present a new concept of integrated biosensing technology using the functionalities of electromagnetic metamaterials and acoustofluidic technology onto a single platform. The new concept of using a single structure to perform microfluidic functions at acoustic frequencies and to detect the characteristics of liquid at microwave frequencies will enable the development of improved lab-on-a-chip devices. As a case study, we demonstrated efficient acoustofluidic functions of mixing and pumping using the designed surface acoustic wave (SAW) device on a $LiNbO_3$ substrate in an experimental setup that also allows the measurement of the electromagnetic characteristics of the interdigitated transducer (IDT) pattern of the same device. We demonstrated microfluidic functions at 10-25 MHz. The device also exhibits electromagnetic resonance at 4.4 GHz with a quality factor value of 294. We showed the device can be used for glucose detection with a good sensitivity of 28 MHz/(mg/ml).

1. Introduction

Wireless health monitoring has become a reality attributed to the development of novel biosensors for a diverse range of applications such as glucometers, blood pressure sensors, and pulse oximeters. Breadth of these applications have been expanding with the development of new sensing and manipulation methods in microsystems. Microsystems technology offers various methods for manipulation of biological fluids for biosampling and preparation purposes, including electromechanical pumping, electrophoresis, and ultrasonic/acoustic actuation. Surface Acoustic Wave (SAW) actuators have been successfully demonstrated for various microfluidic functions including liquid mixing, transport, jetting and nebulisation[1]. SAWs are based on generation of nanometre-scale vibrations on a solid surface. Advantages include freedom from mechanically moving parts and easy-integration into microfluidic systems[2,3]. In addition to conventional SAW devices on rigid substrates, mechanically flexible and bendable thin film-based acoustic wave devices that are suitable for wearable applications have also been demonstrated[4,5].

SAW structures can also be used for sensing based on the piezoelectric effect. The resonant frequency of an acoustic transducer is shifted when an analyte is adsorbed on its surface due to mass loading, or in other cases, changes in elasticity, viscosity or conductivity, thus the frequency of the transducer can be used to detect molecular interactions. However, their major challenges for sensing remain unresolved. The sensitivity of SAW sensors increases significantly with their centre frequencies are increased, favouring smaller devices with resonant frequencies up to GHz levels[6]. Yet, this results in a higher energy attenuation along the interfacing surface with the contacting fluid[7]. In addition, smaller devices require stringent control in manufacturing. As an alternative technology, film bulk acoustic resonators (FBAR) have been used for sensing. The operation principle of the FBAR transducers is based on resonating bulk waves between two electrodes separated with a piezoelectric film layer. FBAR transducers generally favour being smaller, thus are operated at higher frequencies, offering a much higher sensitivity. FBAR devices can be used for liquid sampling but their liquid manipulation and microfluidic function are rather limited compared to that of SAW transducers[5]. Thus, it is very challenging to optimise a single acoustic wave transducer for both sensing and actuation. In addition, the selectivity of the acoustic sensors is

relatively poor, and the resonant frequency is significantly affected by variations in ambient conditions, including non-specific mass loading and temperature[5,6]. Different approaches have been utilised to address these challenges. For example, exciting shear horizontal waves on the surface of the SAW devices or exciting them using later electric fields can significantly reduce the loss in acoustic energy into the liquid environment. Efficient devices using these approaches have been demonstrated for sensing applications[8–10]. Furthermore, combining sensing and actuation capabilities will pave the path for an integrated biosensing platform with efficient sample handling and high precision detection capabilities.

A promising sensing technology with high quality factors at frequencies higher than those of acoustic wave devices is electromagnetic metamaterials. Metamaterials exhibit electromagnetic properties, which are not present in the conventional materials. These include negative values of electric permittivity and magnetic permeability that can be achieved simultaneously[11]. Among different geometrical configurations, split-ring resonators (SRRs) are one of the most common structures for electromagnetic metamaterials. A conventional SRR is simply a ring with a split, which is preferably made of a highly-conductive metal on a dielectric substrate. In addition to their favourable electromagnetic characteristics, SRR devices can be realised in a simple and cost-effective manner with various flexible configurations. An SRR structure electrically forms an *LC* resonator at its magnetic resonance when a circulating resonant current is induced along its surface with the resonant frequency, inductance and capacitance determined by the geometry of the structure. SRR structures in centimetre to millimetre-scale, similar to SAW devices, are usually used for applications in microwave bands. Unlike the conventional types of passive resonators, an SRR structure typically exhibits very sharp resonant behaviour with quality factors larger than 1,000 at microwave frequencies[12]. Owing to their high-quality factors, the change in the resonant frequency of an SRR structure can be effectively used as a sensing mechanism, and it can be induced by a change in dielectric properties of the surrounding medium. Different SRR biosensors have been demonstrated, for which binding of biomolecules on top of an SRR structure alters the device capacitance[13–15]. In addition to their high sensitivity, these structures offer advantages over acoustic wave devices in terms of specificity, e.g., they are not significantly affected by non-specific mass loading and temperature.

In this paper, we, for the first time, introduce a new concept of integrating a SAW device and an electromagnetic metamaterial using a single-electrode structure. The structure is inspired by SRRs with their capability of inducing resonating current for electromagnetic sensing. The SRR-inspired electromagnetic metamaterial structure allows wireless measurements with high quality factors. In addition, the single-electrode structure defines an acoustofluidic device on a piezoelectric substrate. The focus of our concept is to achieve a dual functionality using acoustic transduction and metamaterial-based sensing capable of providing non-invasive, portable, fast, affordable, and accurate biosensors. We report the fluid manipulation capabilities of an acoustic transducer together with its electromagnetic detection capability based on its metamaterial functionality, and successfully demonstrate our device for glucose sensing.

2. Results and Discussion

2.1. Acoustofluidic Characteristics

We have used a SAW device fabricated on a lithium niobate ($LiNbO_3$) substrate. The transducer has curved interdigitated (IDT) electrodes configured in a semi-annular pattern with an outer radius of 4 mm. The period of IDT electrodes is 100 μm. The IDT electrodes were defined using sputtered aluminium and a standard photolithographic lift-off process. We coupled this device with a pair of monopole patch antennas realised on a standard printed circuit board substrate (FR4, glass-reinforced epoxy laminate material) as conceptually shown in Figure 1. The antennas are 26 mm in length and 3 mm in width. We connect the antennas to the ports of a vector network analyser (VNA) to excite the device electromagnetically and to measure the scattering parameters of the device between the antennas. In addition, the IDT pads allow us to excite the SAW device electrically by applying an RF signal for liquid manipulation experiments. During these experiments, we treat the surface of the structure with CYTOP, which is an amorphous fluoropolymer providing water and oil repellency, thus increased hydrophobicity. Figure 1(b) shows the cross-sectional schematic of the device depicting the layers. FR4 and $LiNbO_3$ provide dielectric substrates with permittivity values of 4.3 for FR4 and $\varepsilon_{11}=85,\ \varepsilon_{33}=29.5$ for $LiNbO_3$.

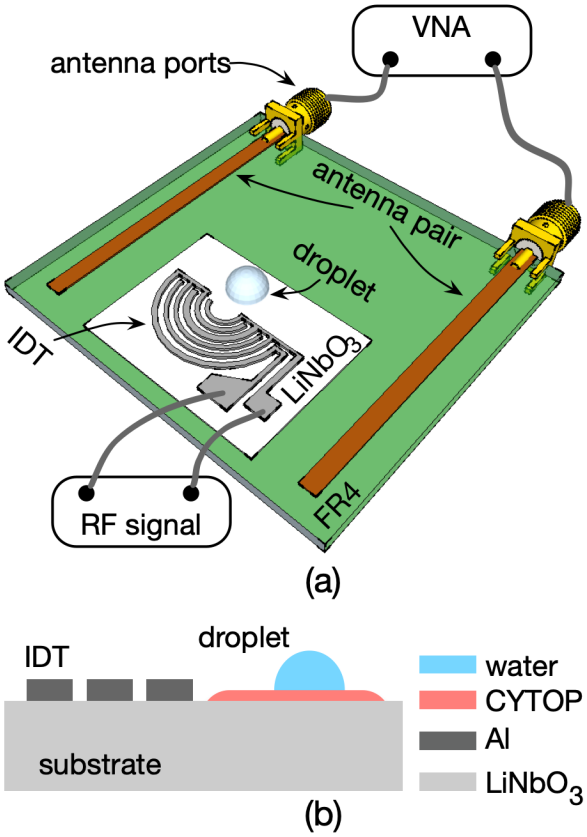

Figure 1. (a) Illustration of a SAW device on a LiNbO3 substrate which is placed on a FR4 substrate including antennas for electromagnetic excitation. (b) Cross-sectional schematic of the device.

We measured the s_{11} (reflection coefficient from the port) spectrum of the SAW device at acoustic frequencies between the ports defined by the IDT pads. We observed four distinct frequencies between 10-25 MHz range (see Figure S1 in Supplementary Materials). The period of the IDT electrodes in the particular device is not constant and has some variation among the finger pairs as shown in Figure S2 in Supplementary Materials. We systematically measured the wavelength and observed a variation between 210 µm and 330 µm. The variation in the wavelength results in distinct fundamental resonant frequencies (see Figure S3 in Supplementary Materials). Among these, we observed the SAW device is efficient at 10.8 and 22 MHz. The wavelength of the IDTs determine the wavelength of the acoustic wave (λ) travelling over the surface, so its ratio to the acoustic wave velocity (v) determines the acoustic resonant frequency ($f = v/\lambda$). On the other hand, the wavelength of the IDTs may alter the

electromagnetic resonant frequency of the structure through the surface capacitance and inductance as explained in the next section.

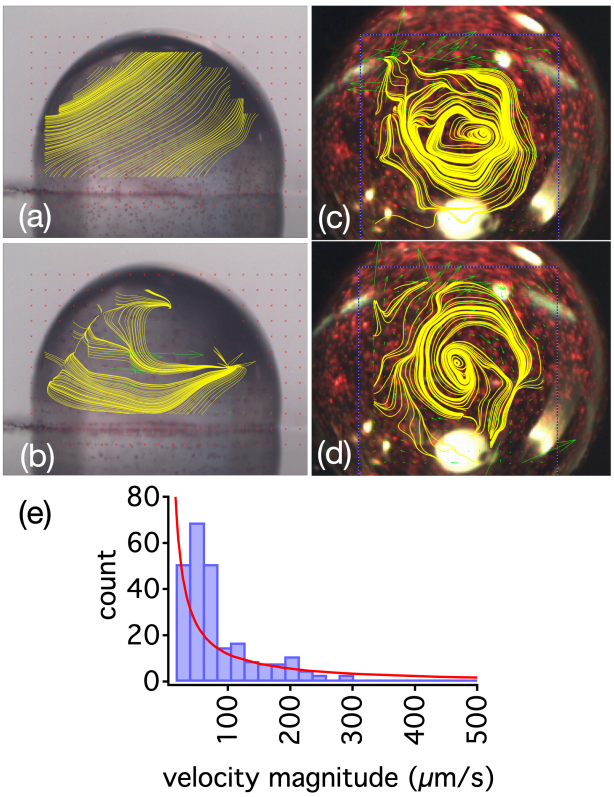

Figure 2. Experimental demonstration of streaming using polystyrene particles inside a droplet with a volume of 2 µL, (a-b) cross-section view (video available in Supplementary Materials, Video S4) and (c-d) top view. (e) The distribution of velocity magnitudes in a time instant shown in subplot-(d).

The curved IDT electrode facilitates a focusing mechanism for the acoustic waves propagating over the substrate. The acoustic wave energy is designed to be focused to the focal point due to the concentration of propagating waves. This was shown to be an effective way of mixing in microfluidics[16]. Consequently, we tested the mixing capability of our SAW device. Figure 2 shows the summary of mixing experiments. First, we treated the surface with a thin layer of CYTOP of ~500 nm thick. Then, we placed a sessile droplet of deionized water with a volume of 2 µL at the focal point of the SAW device. The water droplet comprised of polystyrene microbeads with a diameter of 10 µm. First, we applied an RF signal at 10.8 MHz and observed the motion of polystyrene microbeads using a video camera. Figures 2(a) and 2(b) show the streamlines depicting the trajectories of the particles inside the droplet from a cross-

sectional view. Upon the application of the RF excitation, the particles first started moving at a power of 0.5 W (Figure 2(a)), then gradually formed a steady streaming pattern (Figure 2(b)). We also observed the motion of the particles from the top view at a power of 0.44 W as shown in Figures 2(c) and 2(d). Digital particle image velocimetry results indicate circular mixing patterns in clockwise direction at steady state. We used a digital particle image velocimetry method to calculate the stream velocity inside the droplet[17], and Figure 2(e) shows the calculated distribution of velocity magnitudes of the particles at a steady state of steaming shown in Fig. 2(d).

We then performed liquid pumping experiments using the same SAW device. We placed a droplet of deionized water with a volume of 1 μL on the CYTOP-treated surface along the central axis of the IDT electrodes. Then, we applied RF signals at various power levels and observed the motion of pumped droplets using a video camera. Figure 3(a-d) shows a sequence of snapshots while the droplet was pumped along the surface. Snapshots show consistent droplet shapes in linear translation over the surface. We repeated this experiment at 22 MHz and measured the speed of another droplet with the same volume of 1 μL by varying the power of the RF signal. The pumping of the droplet started at a threshold power of 4.3 W, below which the dominant function was mixing. Figure 3(e) depicts the speed of the droplet as a function of power. Each data point includes 5 different measurements and each error bar denotes the standard deviation of the measured speed. The speed (*mm/s*) increases with power (*W*) within the experimental range following a power law with an exponent of -3.6.

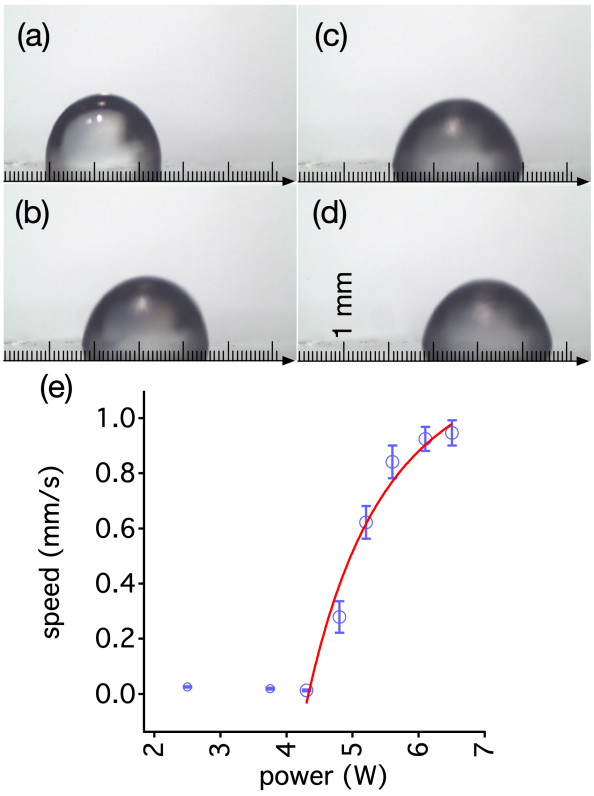

Figure 3. Experimental demonstration of pumping function. Subfigures (a-d) show a sequence of snapshots while a droplet with a volume of 1 µL is pumped along the surface (video available in Supplementary Materials, Video S5). (e) Pumping speed, s, increases with power level, P, following $P \propto s^{3.6}$.

After mixing and pumping experiments, we used the device for liquid jetting experiments. The location of the droplet on the substrate is particularly important for this device since the travelling SAW is focused due to the circular nature of IDT electrodes. We observed that the droplets placed on the focal point can be manipulated vertically. The intensity of SAW is concentrated over a relatively small area at the focal point, so liquid manipulation functions can be implemented effectively. Figures 4(a) to 4(c) show snapshots of a droplet with a volume of 1 µL placed at the focal point of the IDT when a power of 2.9 W at 22 MHz was applied to the IDTs. The droplet did not move from its resting location but was actuated along the vertical axis away from the substrate. We repeated this experiment at different power levels and measured the height of manipulated droplet with increasing power. The maximum height reaches a settled value of 2 mm above its original height at its resting position. The relationship

between the ejected high (h) and the applied power (P) can be described using the following equation for the specific experiment:

$$h = 2.62 - 2.74e^{-\frac{P-0.02}{1.066}} \quad (1)$$

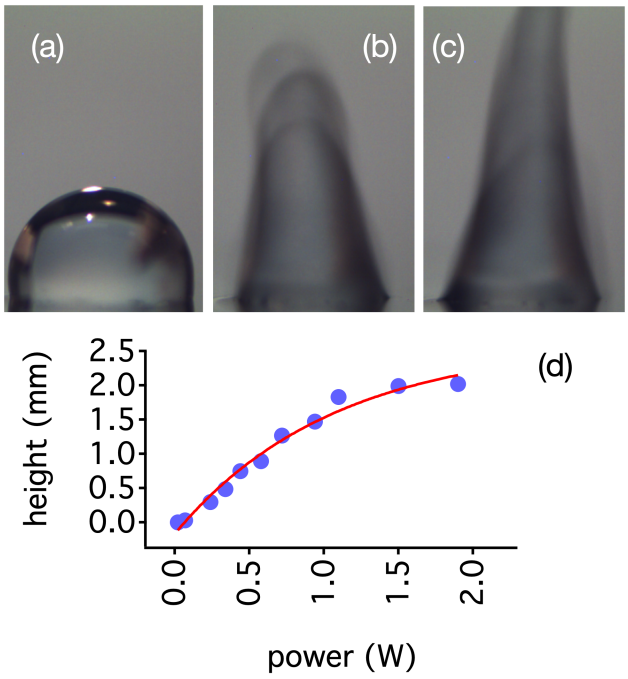

Figure 4. Experimental demonstration of jetting function. Subfigures (a-c) show snapshots while a droplet with a volume of 1 µL is manipulated at a fixed location over the surface (video available in Supplementary Materials, Video S6). (d) The height of the manipulated droplet measured from its original height increases with applied power.

2.2.Electromagnetic Characteristics

In addition to the above microfluidic functionalities, we also characterised electromagnetic properties of the structure. When the transducer is electromagnetically excited using the antenna pair of Figure 1, the magnetic field perpendicular to the SAW IDT supports circulating current at its electromagnetic resonant frequency which is determined by the geometry of the IDTs. The resonant frequency, f_0, and quality factor, Q, of the resonator can be expressed as follows [18].

$$f_0 = \frac{1}{2\pi\sqrt{L_m \cdot (C_m + C_b)}} \quad ; \quad Q = \frac{1}{R}\sqrt{\frac{L_m}{C_m + C_b}} \quad (2)$$

where C_m is the capacitance of the structure and C_b is the effective capacitance of the liquid sample placed within the vicinity of the resonator. L_m is the inductance of the structure and R is the equivalent resistance of the structure and the sample. Since the resonant frequency depends on total capacitance of the structure, which in turn depends on the relative permittivity of the sample, any changes in the physical property of the sample can be observed as changes in f_0 and Q.

Figure 5(a) shows the simulated s_{21} spectrum (transmission coefficient between the ports) of the device. We have used commercially available electromagnetic simulation software (CST Studio Suite, Darmstadt, Germany) for all our simulations. The energy is dissipated across the transducer at the resonance, resulting in a sharp dip signature in the S_{21} spectrum measured between the antenna ports. The spectrum indicates a sharp dip at the resonant frequency of 4.41 GHz with a quality factor of 294. A closer examination of the surface current density at the resonance reveals the pattern of circulating current along the IDT electrodes as shown in Figure 5(b). It is possible to obtain an electromagnetic resonant frequency at 4.41 GHz using a structure with an outer radius of 4 mm, attributed to the SRR-inspired metamaterial configuration that allows the miniaturising of the device to a subwavelength.

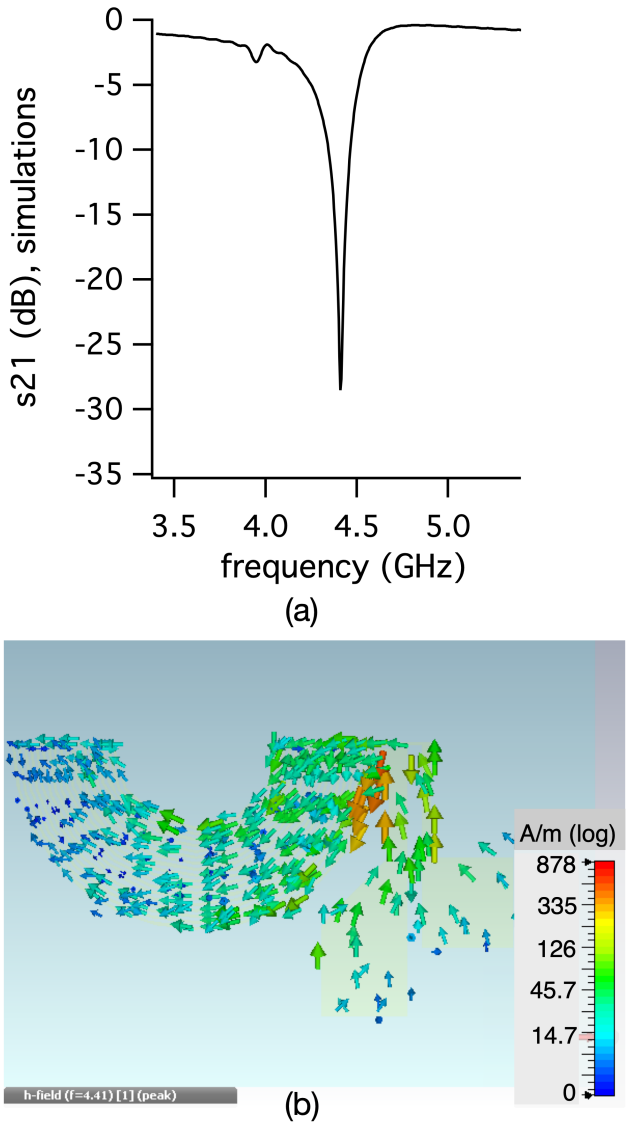

Figure 5. Simulated (a) s21 spectrum of the SAW device, (b) profile of surface current density at the resonance.

Both the circulating current pattern and the electromagnetic resonant frequency of the device are changed when a liquid droplet is placed within the vicinity of the structure. This can be utilised as a sensing mechanism for the location of the droplet. We characterised this mechanism by moving a deionized water droplet with a volume of 2 µl over the surface of the substrate by 4 mm. Figure 6(a) and (b) shows the simulated and experimentally obtained s21 spectra of the sensor while the droplet is moving, respectively. When the droplet was placed 1.5 mm away from the edge of the IDT electrodes, the resonant frequency of the device was dropped to 4 GHz due to the increased value of C_b. Then, the droplet was gradually moved away from the device

along the direction shown in the inset in Figure 6(b). As the droplet was moved away, the value of C_b was decreased, so the resonant frequency of the device was gradually increased. Figure 6(c) shows the simulated and experimentally obtained relationship between the resonant frequency and the droplet distance relative to the edge of the IDT electrodes. During the experiments, we used a vector network analyser to measure the s_{21} spectra of the device between the antenna ports depicted in Figure 1. We observed a linear relationship within the measured displacement range. The slope of the linear fit lines to the experimental and simulated data sets are 28.9 MHz/mm and 35.3 MHz/mm, respectively. The experimentally obtained values of resonant frequency are lower than the simulated ones, which may indicate lower values of dielectric constants in the simulated model as compared with the fabricated device. However, we have used nominal values of the material properties in the material library of the simulator without any fitting parameters. Nevertheless, the simulation results are in a good agreement with that of the experimental ones.

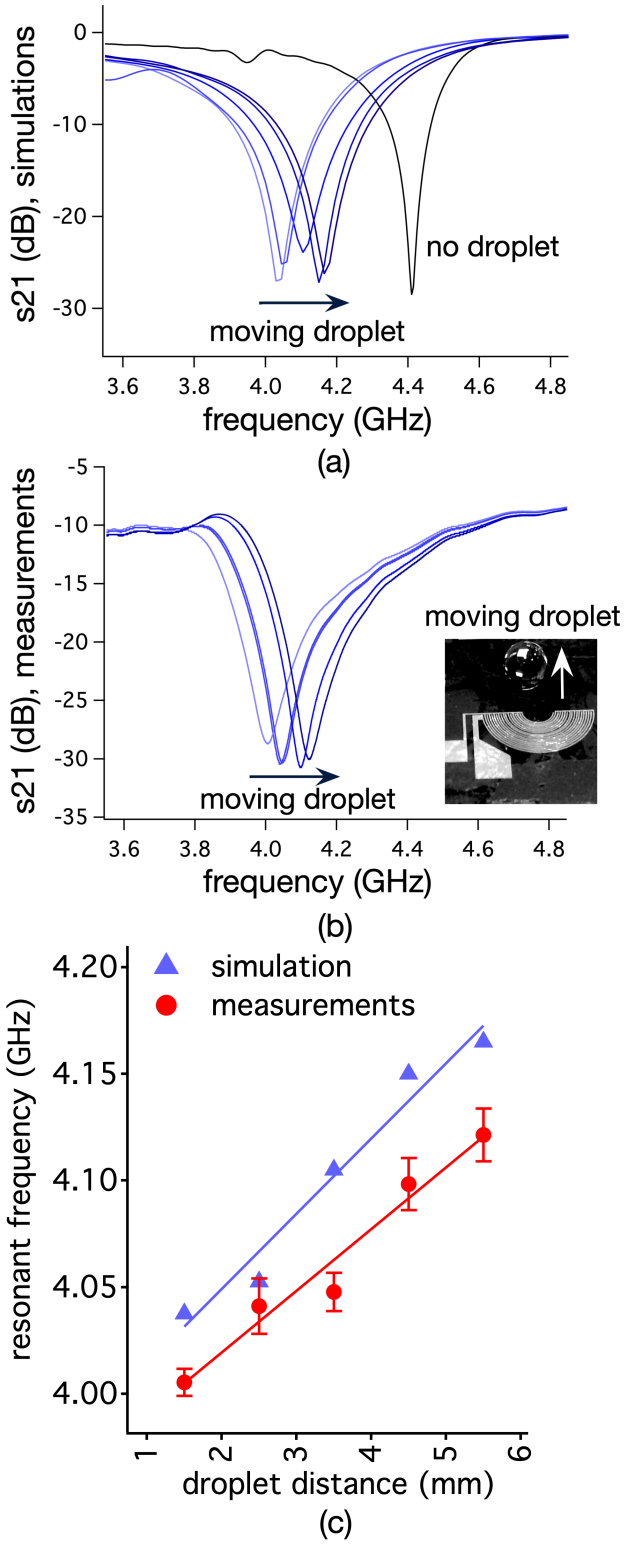

Figure 6. a) Simulated, b) measured s21 spectra of the SAW device while a liquid droplet with a volume of 2 µl is actuated on its substrate. (c) The shift in the resonant frequency of the SAW device due to the movement of a liquid droplet with a volume of 2 µl. The distance of the droplet is measured from the edge of the IDT.

When the location of the droplet is fixed on the substrate, the composition of the droplet can be measured by monitoring the electromagnetic resonant frequency of the device. This approach is simple to implement and relies mainly on the interaction of the sample and the structure under an electromagnetic field. This method is applicable to detect concentration of molecules inside a droplet. In this work, we have used our method for the detection of glucose as an exemplar of the wider applicability of our approach. The permittivity of a droplet of glucose solution decreases with increasing concentration of glucose[19,20]. Therefore, C_b decreases with concentration of glucose, whereas L_m generally stays constant. Thus, the resonant frequency increases with the glucose concentration as demonstrated before[21].

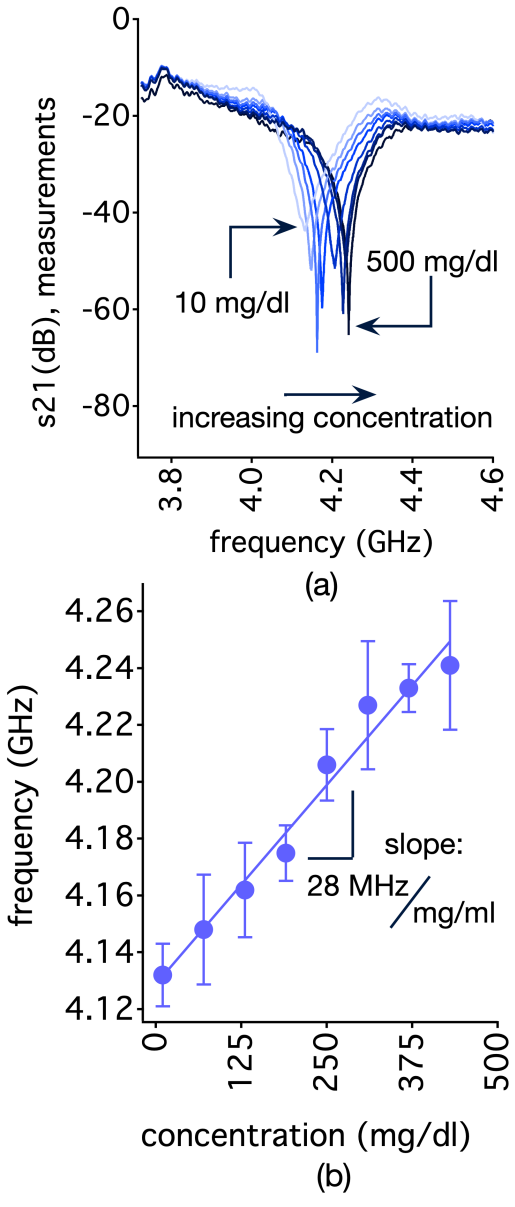

Figure 7. (a) Measured s21 spectra of the device while the concentration of glucose in a 2 µL-droplet is increased. (b) Change in the resonant frequency of the device with concentration of glucose.

We prepared glucose solutions with various concentrations within a physiological range of 10-500 mg/dl in droplets of 2 µl. Then, we placed the droplets sequentially to the same location over the substrate while monitoring the S_{21} spectra of the sensor between the ports of the pair of antennas. Between the application of each droplet, we cleaned the surface using deionized water and dried the sample surface carefully. Figure 7(a) shows the recorded s21 spectra for the samples with different glucose concentrations. The electromagnetic resonant frequency of the transducer increases with glucose concentration as shown in Figure 6(b). We repeated the experiments 10 times and the error bars indicate the standard error of the mean. We observe a linear relationship between the resonant frequency and the concentration within its measurement range with a sensitivity of 28 MHz/(mg/ml), corresponding to 5.05 MHz/mM. This level is comparable to SAW-based acoustofluidic glucose sensors with reported sensitivities of 7.184 MHz/mM[22], 1.589 MHz/mM[23] and 0.93 MHz/log(M)[24]. Based on the above results, we can confirm that this newly developed concept and device can realise the integrated functions of both acoustofluidics and biosensing.

3. Conclusion

In summary, we present a new concept towards the realisation of integrated biosensing platforms. We have successfully demonstrated that a conventional SAW transducer can be employed as a metamaterial-based sensor, the readout of which can be implemented wirelessly using a simple setup.

In this work, we have used a curved IDT SAW device fabricated on a $LiNbO_3$ substrate. We demonstrated liquid mixing, pumping and jetting functions at power levels of 0.2-7 W. In addition to conventional acoustofluidic functionalities, the SAW device acts as an effective electromagnetic metamaterial under electromagnetic excitation. We used a simple setup comprising of a pair of monopole patch antennas on a FR4 substrate for the excitation. The nominal resonant frequency of the device is at 4.41 GHz and the quality factor is 294.

We present the liquid sensing capability of the wireless sensing architecture in two scenarios. Firstly, the droplet motion over the substrate can be measured effectively by monitoring the resonant frequency of the device. Secondly, for a droplet at a fixed location over the substrate, the composition of the droplet can be measured. Consequently, we have used our device for glucose sensing. Our experiments confirm that the concentration of glucose in deionized water droplets with volumes of 2 µl can be measured with a sensitivity of 28 MHz/(mg/ml) within a range of 10-500 mg/dl.

We expect the impact of our work will be beyond the case study with the potential of delivering portable, fast, affordable and accurate monitoring microsystems with intervention capabilities.

Conflicts of interest

There are no conflicts to declare

Acknowledgements

UK Engineering and Physical Sciences Research Council (EPSRC) for support under grant EP/P018998/1.

References

1 J. Friend and L. Y. Yeo, *Rev. Mod. Phys.*, 2011, **83**, 647–704.

2 A. J. Flewitt, J. K. Luo, Y. Q. Fu, L. Garcia-Gancedo, X. Y. Du, J. R. Lu, X. B. Zhao, E. Iborra, M. Ramos and W. I. Milne, *J. Nonnewton. Fluid Mech.*, , DOI:10.1016/j.jnnfm.2014.12.002.

3 G. Destgeer, H. Cho, B. H. Ha, J. H. Jung, J. Park and H. J. Sung, *Lab Chip*, 2016, **16**, 660–667.

4 Y. Q. Fu, J. K. Luo, X. Y. Du, A. J. Flewitt, Y. Li, G. H. Markx, A. J. Walton and W. I. Milne, *Sensors Actuators, B Chem.*, , DOI:10.1016/j.snb.2009.10.010.

5 Y. Q. Fu, J. K. Luo, N. T. Nguyen, A. J. Walton, A. J. Flewitt, X. T. Zu, Y. Li, G. McHale, A. Matthews, E. Iborra, H. Du and W. I. Milne, *Prog. Mater. Sci.*, 2017.

6 A. Mujahid and F. L. Dickert, *Sensors (Switzerland)*, 2017, 17.

7 X. Ding, P. Li, S.-C. S. Lin, Z. S. Stratton, N. Nama, F. Guo, D. Slotcavage, X. Mao, J. Shi, F. Costanzo and T. J. Huang, *Lab Chip*, 2013, **13**, 3626.

8 O. I. Guliy, B. D. Zaitsev, I. E. Kuznetsova, A. M. Shikhabudinov, L. Y. Matora, S. S. Makarihina and O. V. Ignatov, *Microbiology*, 2013, **82**, 215–223.

9 I. Guliy, B. D. Zaitsev, I. A. Borodina, Shikhabudinov, A. A. Teplykh, S. A. Staroverov and A. S. Fomin, *Talanta*, 2018, **178**, 569–576.

10 F. Bender, R. E. Mohler, A. J. Ricco and F. Josse, *Anal. Chem.*, 2014, **86**, 1794–1799.

11 D. Schurig, J. J. Mock, B. J. Justice, S. A. Cummer, J. B. Pendry, A. F. Starr and D. R. Smith, *Science (80-.).*, 2006, **314**, 977–980.

12 H. Torun, S. Sadeghzadeh and A. D. Yalcinkaya, *Rev. Sci. Instrum.*, , DOI:10.1063/1.4825347.

13 H. J. Lee, J. H. Lee, H. S. Moon, I. S. Jang, J. S. Choi, J. G. Yook and H. Il Jung, *Sensors Actuators, B Chem.*, 2012, **169**, 26–31.

14 W. Withayachumnankul, K. Jaruwongrungsee, A. Tuantranont, C. Fumeaux and D. Abbott, *Sensors Actuators, A Phys.*, 2013, **189**, 233–237.

15 A. Salim and S. Lim, *Sensors (Switzerland)*, , DOI:10.3390/s16111802.

16 R. Shilton, M. K. Tan, L. Y. Yeo and J. R. Friend, *J. Appl. Phys.*, , DOI:10.1063/1.2951467.

17 W. Thielicke and E. J. Stamhuis, *J. Open Res. Softw.*, , DOI:10.5334/jors.bl.

18 H. Torun, F. Cagri Top, G. Dundar and A. D. Yalcinkaya, *J. Appl. Phys.*, , DOI:10.1063/1.4896261.

19 V. Turgul and I. Kale, *IEEE Int. Instrum. Meas. Technol. Conf. Proc.*, 2016, 1–5.

20 E. Topsakal, T. Karacolak and E. C. Moreland, *2011 URSI Gen. Assem. Sci. Symp.*, 2011, 1–4.

21 B. Camli, E. Altinagac, H. Kizil, H. Torun, G. Dundar and A. D. Yalcinkaya, *Proc.* , 2018, 2.

22 J. Luo, P. Luo, M. Xie, K. Du, B. Zhao, F. Pan, P. Fan, F. Zeng, D. Zhang, Z. Zheng and G. Liang, *Biosens. Bioelectron.*, 2013, **49**, 512–518.

23 J. Luo, M. Xie, P. Luo, B. Zhao, K. Du and P. Fan, *Mater. Lett.*, 2014, **130**, 14–15.

24 F. F. Chou and J. S. Shih, *Sensors Actuators, B Chem.*, 2008, **129**, 176–183.

SUPPLEMENTARY MATERIALS

A Fully Integrated Biosensing Platform Combining Acoustofluidics and Electromagnetic Metamaterials

S. Zahertar,[1] Y. Wang,[2] R.Tao,[1] J. Xie,[2] Y.Q. Fu,[1] H. Torun[1,*]

[1]Faculty of Engineering and Environment, Northumbria University, Newcastle upon Tyne, NE1 8ST, UK

[2] The State Key Laboratory of Fluid Power and Mechatronic Systems, Zhejiang University, Hangzhou 310027, China

* Corresponding author: Hamdi Torun, hamdi.torun@northumbria.ac.uk

Number of Pages: 1–3
Number of Figures: S1–S3
Number of tables: S4-S6

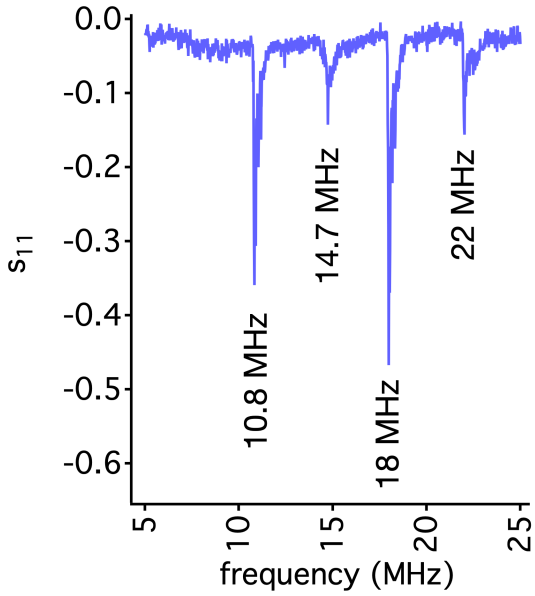

Figure S1: S_{11} spectrum of the SAW device at acoustic frequencies. We used a network analyser to measure the spectrum between the ports defined by the pads of the IDT electrodes.

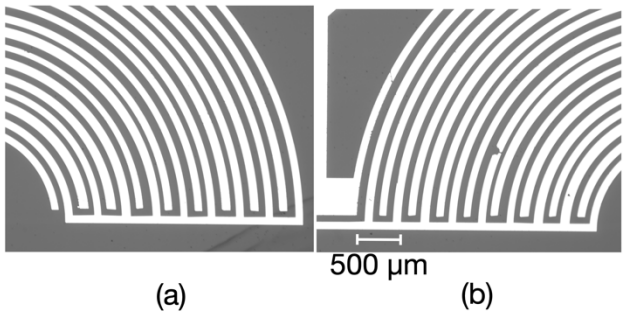

Figure S2: Micrographs of two sections of the IDT electrodes illustrating the variations in the finger widths of the IDT electrodes.

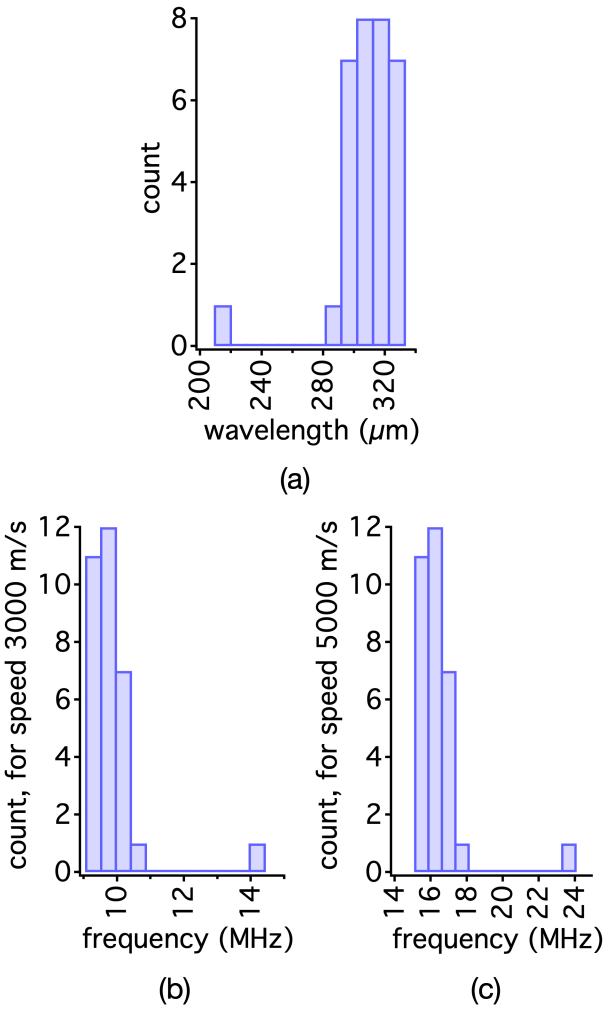

Figure S3: (a) Histogram of the wavelength measured between consecutive pairs of fingers. Histogram of the calculated resonant frequencies for acoustic speeds of (b) 3000 m/s and (c) 5000 m/s. We measured the finger widths along four different radial axes on the curved IDT to generate statistics. The variation in finger width results in different frequencies observed in s_{11} spectrum as shown in Figure S1.

Video S4: A sample video showing a typical mixing experiment where a droplet with a volume of 2 µL including polystyrene particles with a diameter of 10 µm was used.

Video S5: A sample video showing a typical pumping experiment where a droplet with a volume of 1 µL was pumped over the substrate.

Video S6: A sample video showing an experiment where the droplet was manipulated away from the substrate.